Journal of Sound and Vibration (2001) **240**(3), 545–565
doi:10.1006/jsvi.2000.3248, available online at http://www.idealibrary.com on IDEAL®

IDENTIFICATION OF DAMPING MATRICES FROM MEASURED FREQUENCY RESPONSE FUNCTIONS

J.-H. Lee and J. Kim

Structural Dynamics Research Laboratory, Mechanical Engineering Department, University of Cincinnati, Cincinnati, OH 45221-0072, *U.S.A. E-mail: jay.kim@uc.edu*

(*Received* 14 *January* 2000, *and in final form* 17 *July* 2000)

An improved method to identify damping characteristics of a dynamic system is developed. The method identifies damping characteristics of the system in matrix forms directly from its measured frequency response functions. Each different damping mechanism is identified in a distinct matrix. Theoretical validation and related error analysis are conducted by applying the method to a simple lumped parameter system. The method is implemented experimentally to a thin beam of two different damping configurations. The experimental results demonstrate that the method will work well with realistic problems. Important advantages of the method and potential applications are explained.

1. INTRODUCTION

1.1. MOTIVATION OF THE WORK

Damping parameters have been of relatively minor concern to test engineers when compared to other modal parameters. Often damping characteristics are identified as modal damping ratios, which represent combined effects of many different damping mechanisms without any spatial information. An experimental method is developed in this work to identify damping characteristics of a dynamic system in damping matrices so that types and spatial distributions of the damping can be identified.

Identifying the damping in matrix form has an important potential application to hybrid modelling of a mechanical system. In the hybrid modelling, the mass and stiffness matrices are formulated by the finite element method (FEM) and the damping matrices are formulated experimentally, which are then combined to obtain the system equation. The advantage of such an approach is easily understood if it is considered that the mass and stiffness matrices are formulated quite accurately, but not the damping matrices by FEM.

1.2. RELATED PREVIOUS WORKS

Most techniques that have been proposed for damping matrices identification use frequency response functions (FRFs) indirectly, in which modal parameters such as natural frequencies and modes are extracted from the FRF first, then damping matrices are formulated using these modal parameters. Pilkey and Inman [1] proposed an iterative approach to identify the viscous damping matrix. The method is based on the inverse

0022-460X/01/080545 + 21 $35.00/0

eigenvalue problem concept, in which the damping matrix is constructed from the eigenvalues and eigenvectors. Lancaster [2] developed an inverse method to calculate the modal coefficient matrices. In his approach, the mass, viscous damping and stiffness matrices of a system are computed from given eigenvalues and eigenvectors. Because these methods use eigenvalues and eigenvectors, data once processed from FRFs, they are considered more susceptible to measurement noises and errors. Obviously, abundant literature is found on the general modal identification subject. Ebersbach and Irretier [3] studied the application of modal parameter estimation using frequency domain algorithms to identify eigenvalues and eigenvectors from the measured FRFs of a structure. Allemang and Brown [4] presented a unified matrix polynomial approach to modal identification in order to identify eigenvalues and eigenvectors of a structure.

Chen and Tsuei [5–7] studied the effect of parameter identification on modelling of viscous and structural damping. They proposed to use the normal FRFs extracted from the complex FRF and the singular-value decomposition (SVD) method to identify the damping matrices. Their work was limited to theoretical study without any experimental implementation. The theoretical scheme of the method developed in this work generally follows the method proposed by Chen and Tsuei. The method was generalized so that it can be applied to the experimental multi-input–multi-output (MIMO) systems to identify and distinguish various mechanisms in distinct matrices directly from the measured FRFs.

1.3. OVERVIEW OF THE WORK

In this paper, a new theoretical procedure for the damping identification is discussed. Verification of the method is made by applying the method to a simple three degree-of-freedom (3 d.o.f.) lumped parameter system that has both the viscous and structural damping. The effect of the noise in the measured FRFs is also studied using this example. The method is then applied to an experimental example to confirm its practical value in real engineering problems. A thin beam with clamped boundary conditions with two damping configurations is used in the experiment. It is shown that the identification result explains the different configurations very well; for example, the viscous damping matrix becomes relatively large when a viscous damper is added to the beam.

2. THEORY OF DAMPING MATRICES IDENTIFICATION

2.1. THEORETICAL DEVELOPMENT

For a harmonic excitation, the equation of motion of a dynamic system of n d.o.f. is represented by

$$M\ddot{x}(t) + C\dot{x}(t) + (\mathrm{j}D + K)x(t) = F(\omega)\mathrm{e}^{\mathrm{j}\omega t}, \tag{1}$$

where M, C, D and K are $n \times n$ matrices representing the mass, viscous damping, structural damping and stiffness of the system, respectively, $\mathrm{j} = \sqrt{-1}$, and $x(t)$ and $f(t)$ are $n \times 1$ vectors representing the displacements and the applied forces.

Since $x(t) = X(\omega)\mathrm{e}^{\mathrm{j}\omega t}$, equation (1) becomes

$$[K - M\omega^2]X(\omega) + \mathrm{j}\omega CX(\omega) + \mathrm{j}DX(\omega) = F(\omega). \tag{2}$$

Identifying the normal FRF $H^N(\omega)$ such as

$$H^N(\omega) = [K - M\omega^2]^{-1}, \tag{3}$$

equation (2) is written as

$$[H^N(\omega)]^{-1} X(\omega) + (\mathrm{j}\omega C + \mathrm{j}D)X(\omega) = F(\omega). \tag{4}$$

Pre-multiplying equation (4) by $H^N(\omega)$ results in

$$X(\omega) + \mathrm{j}H^N(\omega)(\omega C + D)X(\omega) = H^N(\omega)F(\omega). \tag{5}$$

Further, if we define a real matrix $G(\omega)$ as Chen and Tsuei [5] did,

$$G(\omega) \equiv H^N(\omega)(\omega C + D). \tag{6}$$

Then, equation (5) becomes

$$[I + \mathrm{j}G(\omega)]X(\omega) = H^N(\omega)F(\omega), \tag{7}$$

where I is an identity matrix.

The displacement vector $X(\omega)$ in equation (7) is related to the input force and the complex FRF $H^C(\omega)$ by

$$X(\omega) = H^C(\omega)F(\omega) = [H_R^C(\omega) + \mathrm{j}H_I^C(\omega)]F(\omega), \tag{8}$$

where $H_R^C(\omega)$ and $H_I^C(\omega)$ represent, respectively, the real and imaginary parts of $H^C(\omega)$. The complex FRF $H^C(\omega)$ can be measured, therefore is the known information. Substituting equation (8) into equation (7), one obtains

$$(I + \mathrm{j}G(\omega))(H_R^C(\omega) + \mathrm{j}H_I^C(\omega))F(\omega) = H^N(\omega)F(\omega). \tag{9}$$

From equation (9), it is easily seen that

$$(I + \mathrm{j}G(\omega))(H_R^C(\omega) + \mathrm{j}H_I^C) = H^N. \tag{10}$$

Since equation (10) is a complex equation, two equations are obtained from its real and imaginary parts:

$$H^N(\omega) = H_R^C(\omega) - G(\omega)H_I^C(\omega), \quad G(\omega)H_R^C(\omega) = -H_I^C(\omega). \tag{11, 12}$$

From equation (12), $G(\omega)$ is expressed in terms of the known function $H^C(\omega)$:

$$G(\omega) = -H_I^C(\omega)H_R^C(\omega)^{-1}. \tag{13}$$

Equation (13) can be ill-conditioned when the matrix is inverted. A small error in the estimation of the real part of the FRF ($H_R^C(\omega)$) may result in large errors in identified damping matrices. Over-determining the system equation and more accurate phase matching of the force and acceleration transducers will alleviate this problem.

The normal FRF $H^N(\omega)$ is obtained by substituting equation (13) into equation (11):

$$H^N(\omega) = H_R^C(\omega) + H_I^C(\omega)H_R^C(\omega)^{-1}H_I^C(\omega). \tag{14}$$

Because $G(\omega)$ and $H^N(\omega)$ are known now, equation (6) can be written as

$$[\omega H^N(\omega) H^N(\omega)] \begin{bmatrix} C \\ D \end{bmatrix} = G(\omega). \tag{15}$$

Equation (15) can be used to solve the damping matrices C and D, which are the objectives of the identification. Thus, the damping matrices identification procedure can be summarized as follows: (1) obtain the complex FRF matrix $H^C(\omega)$ from measurement; (2) find the normal FRF matrix $H^N(\omega)$ from equation (14); (3) find $G(\omega)$ from equation (13); and (4) find C and D from equation (15).

2.2. EXPERIMENTAL DAMPING IDENTIFICATION PROCEDURE

Equation (15) can be applied at more frequencies than necessary (two are the minimum necessary) to make the equation over-determined. If k different frequencies are used, the equation becomes

$$\begin{bmatrix} \omega_1[H^N(\omega_1)]_{n\times n} & [H^N(\omega_1)]_{n\times n} \\ \omega_2[H^N(\omega_2)]_{n\times n} & [H^N(\omega_2)]_{n\times n} \\ \vdots & \vdots \\ \omega_k[H^N(\omega_k)]_{n\times n} & [H^N(\omega_k)]_{n\times n} \end{bmatrix}_{kn\times 2n} \begin{bmatrix} [C]_{n\times n} \\ [D]_{n\times n} \end{bmatrix}_{2n\times n} = \begin{bmatrix} [G(\omega_1)]_{n\times n} \\ [G(\omega_2)]_{n\times n} \\ \vdots \\ [G(\omega_k)]_{n\times n} \end{bmatrix}_{kn\times n}. \tag{16}$$

The damping matrices can be found by the pseudo-inverse procedure:

$$\begin{bmatrix} [C]_{n\times n} \\ [D]_{n\times n} \end{bmatrix}_{2n\times n} = \begin{bmatrix} \omega_1[H^N(\omega_1)]_{n\times n} & [H^N(\omega_1)]_{n\times n} \\ \omega_2[H^N(\omega_2)]_{n\times n} & [H^N(\omega_2)]_{n\times n} \\ \vdots & \vdots \\ \omega_k[H^N(\omega_k)]_{n\times n} & [H^N(\omega_k)]_{n\times n} \end{bmatrix}^{+}_{kn\times 2n} \begin{bmatrix} [G(\omega_1)]_{n\times n} \\ [G(\omega_2)]_{n\times n} \\ \vdots \\ [G(\omega_k)]_{n\times n} \end{bmatrix}_{kn\times n}, \tag{17}$$

where $+$ means the pseudo-inverse of the matrix.

The measured FRF matrix $H^C(\omega)$ is the only necessary information to obtain the damping matrices $[C]$ and $[D]$ to solve equation (17). The dimension of the complex FRF matrix $H^C(\omega)$, therefore the dimension of damping matrices being identified, is determined by the d.o.f.s of the experimental model. For example, if $H^C(\omega)$ is obtained as a 4×4 matrix, the damping matrices will be identified as 4×4 matrices. In such a case, 16 FRFs between 4 input and 4 output points, or 10 FRFs if Maxwell's reciprocity theorem is applied, have to be measured.

When the method is applied to build a FEM/experimental hybrid model, in which the mass and stiffness matrices are obtained from the FEM formulation [8, 9] and the damping matrices are obtained experimentally by this method, the FEM model usually has a much finer mesh than the experimental model. Moreover, some d.o.f.s of the FEM model, such as the rotational or in-plane d.o.f.s, cannot be measured in the experiment, which will force one to expand the measured damping matrices. Therefore, it will be convenient to choose the nodal points of the experimental model as a sub-set of those of the FEM model.

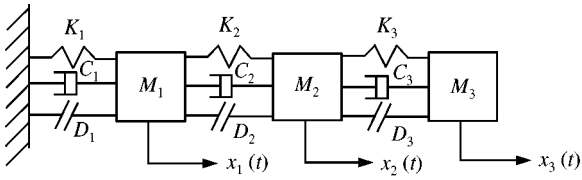

Figure 1. 3 d.o.f. lumped parameter system.

TABLE 1

Matrices of the 3 d.o.f. lumped parameter system

Mass matrix (kg) [M]			Viscous damping matrix (N s/m) [C]			Stiffness matrix (N/m) [K]			Structural damping matrix (N/m) [D]		
10	0	0	5	− 3	0	5000	− 3000	0	250	− 150	0
0	14	0	− 3	5·5	− 2·5	− 3000	5500	− 2500	− 150	350	− 200
0	0	12	0	− 2·5	2·5	0	− 2500	2500	0	− 200	200

3. THEORETICAL VALIDATION OF THE PROCEDURE

The 3-d.o.f. system shown in Figure 1 is defined by the lumped masses m_1, m_2 and m_3 of 10, 14 and 12 kg, and the spring constants k_1, k_2, and k_3 of 2000, 3000 and 2500 N/m, the viscous damping coefficients c_1, c_2, and c_3 of 2, 3 and 2·5 N s/m, and the structural damping coefficients d_1, d_2 and d_3 of 100, 150 and 200 N/m respectively. The elements of the mass, viscous damping, stiffness and structural damping matrices of the system in Figure 1 are calculated as in Table 1. It is noted that the mass and stiffness matrices are shown only for reference, and are not necessary in the damping identification procedure.

Because the system has 3 d.o.f.s, nine FRFs are calculated at each frequency, forming a 3×3 FRF matrix of a function of frequency. Then, assuming that these FRFs are available from measurement, the procedure developed in the previous section is applied to find the damping matrices. Obviously, the damping matrices shown in Table 1 have to be identified within numerical errors by the procedure.

Table 2 shows the viscous and structural damping matrices identified by the proposed method when the calculated FRFs are used without adding any noise. Two cases are shown in the table. Case A is the identification result obtained by modelling only the viscous damping, and case B is the result when both the viscous and structural damping effects are modelled. Correct matrices in the table stand for the theoretically formulated damping matrices. Case B shows that the original damping matrices are identified exactly, which means the identification algorithm is valid. In case A, the viscous damping matrix is identified differently compared to the original matrix, because the matrix represents both the viscous and structural damping effects. Figure 2 compares FRFs reconstructed using the identified damping matrices corresponding to cases A and B, and the mass and stiffness matrices. As it is seen, the two FRFs are virtually indistinguishable, which justifies the common practice of using the concept of the equivalent viscous damping to represent the combined effect of all damping mechanisms in lightly damped systems.

TABLE 2

Estimated damping matrices from FRFs with 0% noise

Estimation method	Viscous damping [C]			Structural damping [D]		
Simulation data	5	− 3	0	250	− 150	0
	− 3	5·5	− 2·5	− 150	350	− 200
	0	− 2·5	2·5	0	− 200	200
Case A Viscous damping model	15·6	− 6·5	− 1·1	—	—	—
	− 7·0	20·2	− 9·4	—	—	—
	− 0·7	− 11·4	14.6	—	—	—
Case B Viscous and structural damping model	5	− 3	0	250	− 150	0
	− 3	5·5	2·5	− 150	350	− 200
	0	− 2·5	2·5	0	− 200	200

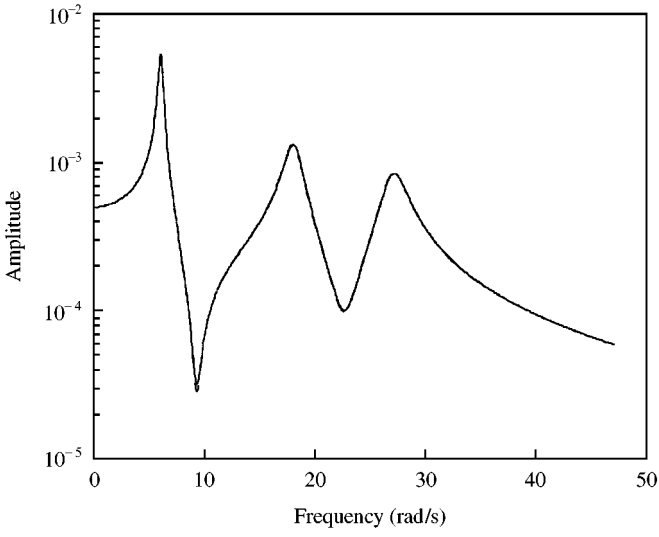

Figure 2. Comparisons of the reconstructed FRFs of 3 d.o.f. lumped mass system: (- - - -), viscous damping model; (——), viscous and structural damping model.

The effect of the measurement noise on the accuracy of the identification result can be studied by using FRFs mixed with various levels of noise. For this purpose, FRFs are transformed to the time domain using the inverse Fourier transform (IFT) [10], which result in impulse response functions. A random noise is added to these time functions, which are transformed back to the frequency domain to obtain FRFs contaminated with the noise. Figures 3 and 4 show H_{22}, before and after 1% random noise (based on the r.m.s value) is added. Table 3 shows the identification result obtained using the FRFs with 1% random noise. Again, case A is the identified result obtained using only the viscous damping matrix and case B is the result obtained using both damping matrices. Figure 5 compares the two impulse response functions reconstructed from the identified damping matrices A and B and the mass and

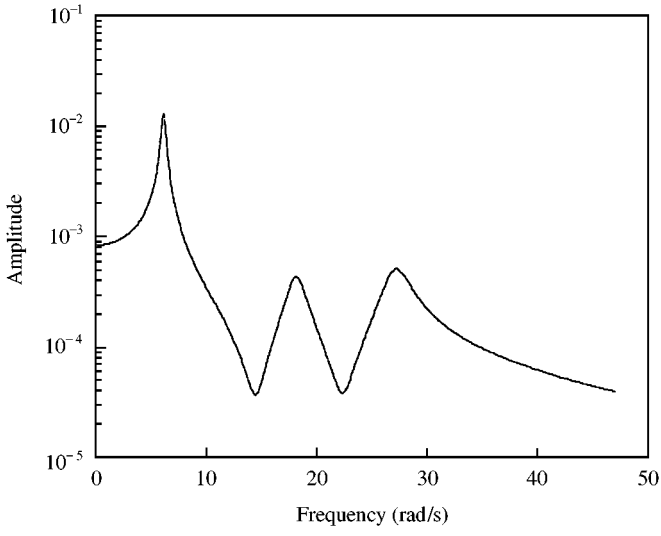

Figure 3. FRF H_{22} of 3 d.o.f. lumped parameter system.

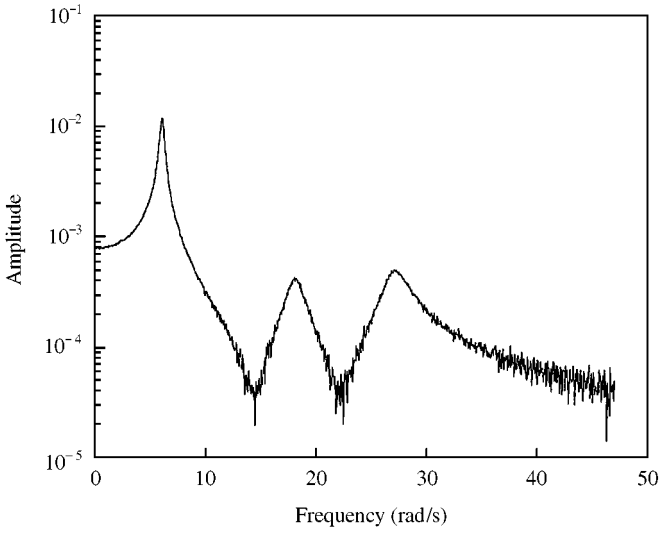

Figure 4. FRF H_{22} of 3 d.o.f. lumped parameter system after 1% noise is added.

stiffness matrices in Table 1. Again, two impulse response functions are virtually indistinguishable. Table 3 and Figure 5 show that the damping matrices are identified accurately despite the 1% noise added to the FRFs.

4. STUDY OF ERROR DUE TO THE NOISE IN FRFS

4.1. RELATIVE MAGNITUDE OF DIFFERENT DAMPING MECHANISMS

It is expected that the effect of the noise on the accuracy of the damping identification will be dependent not only on the noise level but also on the magnitude of the damping.

TABLE 3

Estimated damping matrices from FRFs with 1% noise

Estimation method	Viscous damping [C]			Structural damping [D]		
Simulation data	5	− 3	0	250	− 150	0
	− 3	5·5	− 2·5	− 150	350	− 200
	0	− 2·5	2·5	0	− 200	200
Case A	15·6	− 6·5	− 1·1	—	—	—
Viscous damping	− 7·0	20·2	− 9·4	—	—	—
model	− 0·7	− 11·4	14.6	—	—	—
Case B	5·0	− 3·0	0·0	249·4	− 149·3	0·1
Viscous and structural	− 2·9	5·5	− 2·4	− 149·9	348·5	− 199·5
damping model	0·0	− 2·5	2·5	0·1	− 199·1	199·2

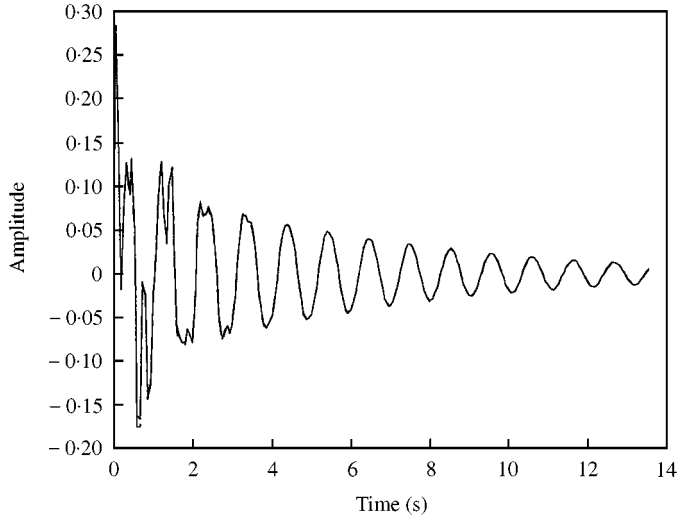

Figure 5. Comparisons of the impulse response functions reconstructed from FRFs with 1% noise: (- - - -), viscous damping model; (——), viscous and structural damping model.

For example, if the structure is heavily damped, the objects of the identification (elements of the damping matrices) are large, therefore the accuracy of the identification will be less sensitive to the noise level. Therefore, it is necessary to cross-compare the magnitudes of the damping and the noise level. Comparing the noise level with the damping ratio makes sense because both are non-dimensional parameters. For example, we may say that a 2% noise is large when compared with a 1% damping ratio. Since the damping ratio is a concept based on the proportional viscous damping that does not have any spatial information, it is necessary to define a new concept to assess the relative magnitude of the elements of general damping matrices.

The damping forces induced by the viscous and structural damping mechanisms associated with specific d.o.f. i and j can be considered as ωC_{ij} and D_{ij}. Therefore, if one

defines a frequency matrix such as

$$[\omega_{ij}] = \left[\frac{D_{ij}}{C_{ij}}\right], \tag{18}$$

each element of this matrix represents the frequency below which the structural damping effect is bigger than that of the viscous damping. For example, ω_{11} of the system in our example is found to be 50 rad/s, which means that below 50 rad/s the effect of the structural damping is a more dominant energy dissipation mechanism for the motion induced at node 1 by the excitation force applied at node 1. Figures 6 and 7 show interesting

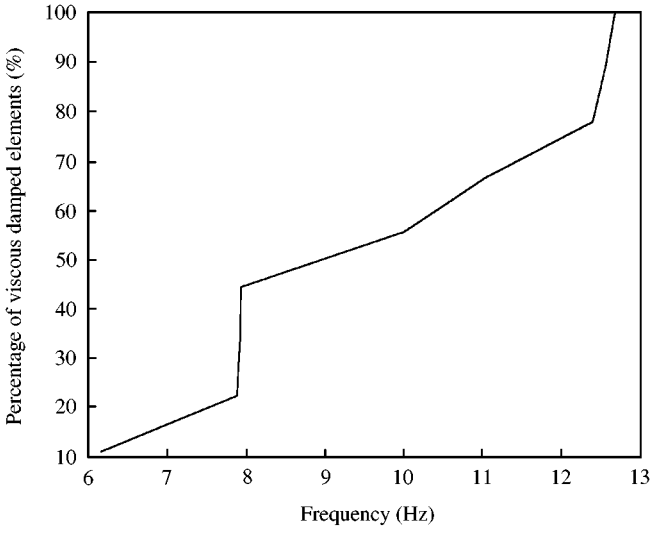

Figure 6. Viscous damping index.

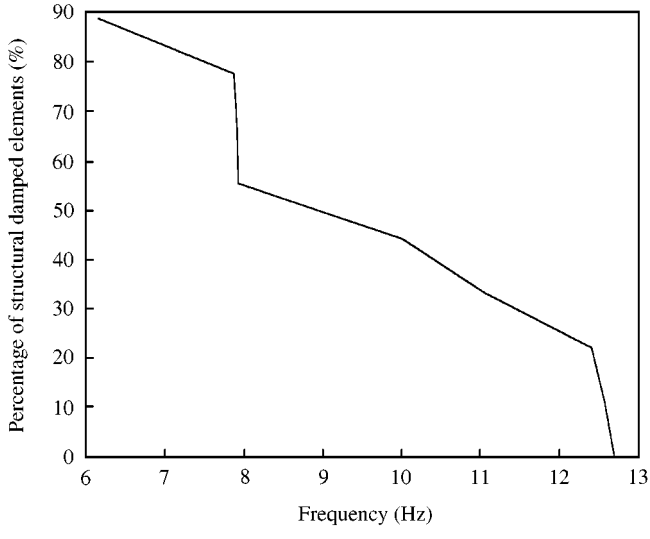

Figure 7. Structural damping index.

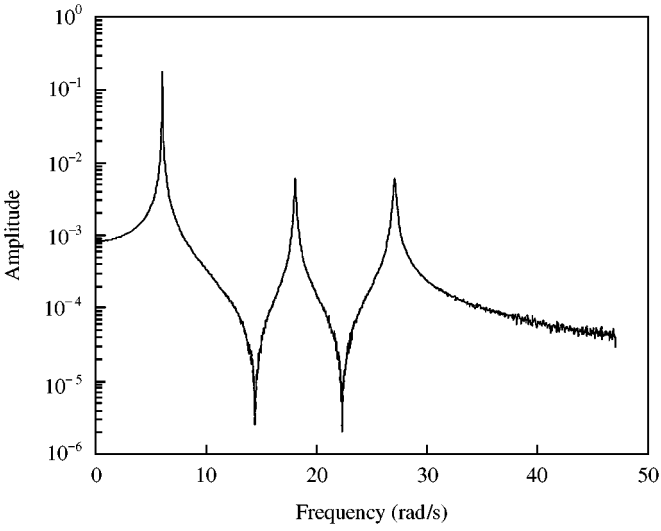

Figure 8. FRF of the system with 0·1% viscous and structural damping and 0·1% noise: (- - - - -), without noise; (——), 0·1% noise.

concepts: the viscous damping index and the structural damping index, which are calculated for the system being studied. Figure 6 (Figure 7) plots the percentage of the elements of the matrix $[\omega_{ij}]$, whose values are lower (higher) than the frequency used as the abscissa. Therefore, for instance, the structural (viscous) damping index is 45% (55%) at 10 Hz in Figure 7, which can be interpreted as approximately 45% (55%) of the system d.o.f.s (4 out of 9 elements in this case) is damped more structurally than viscously. Therefore, from Figures 6 and 7, it can be said that at or above 11 Hz the system is damped primarily by the viscous damping mechanism, and at or below 8 Hz by the structural damping. The frequency range in between may be considered as the transition range.

Now, the concept of the damping ratio [11] is generalized. The elements of the viscous and structural damping matrices are defined in terms of the damping ratio as

$$c_{ij} = 2 \times \zeta_{ij} \times \sqrt{m_{ij} \times k_{ij}}, \quad d_{ij} = c_{ij} \times \omega_{ij}, \quad i, j = 1, 2, 3. \tag{19, 20}$$

The above equations are used to relate the general damping matrices to the damping ratio. For example, 1% viscous damping matrix can be determined by equation (19) using $\zeta_{ij} = 0{\cdot}01$. Then, using the viscous damping elements derived as such, 1% structural damping elements are determined by equation (20). Figure 8 compares H_{22} obtained for the system with 0·1% structural and viscous damping defined in this way with 0·1 and 0% noise.

4.2. STUDY OF NOISE EFFECT

The 3-d.o.f. systems with the same M and K matrices but with two different levels of damping ratios, 0·1 and 0·5%, are considered. For each case, nine FRFs

are calculated, to which three levels of the random noises, 0·1, 0·5 and 1%, are added. This results in six combinations of different noise levels relative to the damping levels. For example, the combination of 0·1% damping and 1% noise represents a system, which has a very small damping, and whose measured FRFs are significantly tainted with noises. In this case, an accurate identification is not expected. Further, an error vector is defined, whose each element is the difference between the exact value and the identified value divided by the largest element of the damping matrix. For this example, which has nine matrix elements, the error vector is defined in % units:

$$\begin{Bmatrix} E_1 \\ E_2 \\ E_3 \\ E_4 \\ E_5 \\ E_6 \\ E_7 \\ E_8 \\ E_9 \end{Bmatrix} = \begin{Bmatrix} (c_{11N} - c_{11}) \\ (c_{12N} - c_{12}) \\ (c_{13N} - c_{13}) \\ (c_{21N} - c_{21}) \\ (c_{22N} - c_{22}) \\ (c_{23N} - c_{23}) \\ (c_{31N} - c_{31}) \\ (c_{32N} - c_{32}) \\ (c_{33N} - c_{33}) \end{Bmatrix}_{Extracted} \times \frac{100}{\max([c_{ij}])}, \tag{21}$$

where, subscript N indicates the exact value.

Figure 9 shows the identification error defined as above for the case with 0·1% damping and 0·1% noise. When equations (17) is applied to identify damping matrices, one can use FRFs at frequencies over the entire range or at frequencies around the resonance peaks. The result obtained using the entire frequency range is marked as "entire frequency range" and that obtained using the frequencies near the resonance frequencies is marked as "peak band" in Figure 9 and other figures to follow. Considering the fact that the damping effect is more pronounced at frequencies near the resonance peaks, it was expected that peak band cases would provide better results. This turns out to be

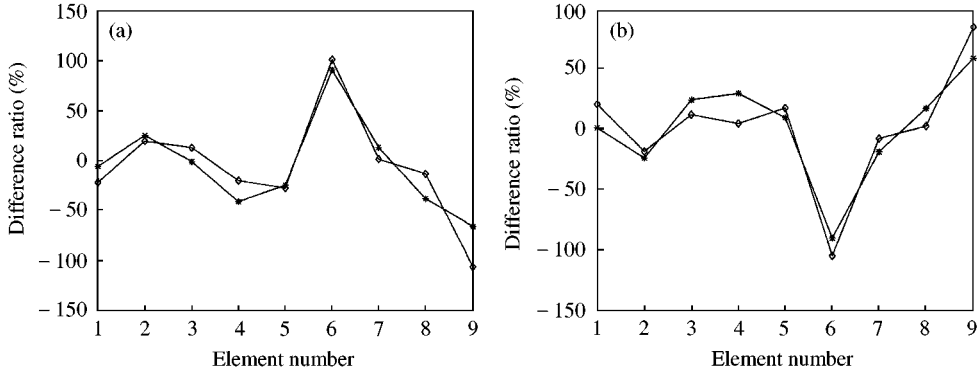

Figure 9. Error ratio diagram of a system with 0·1% damping and 0·1% noise. (a) The identified viscous damping: (—∗—), peak band; (—◇—), entire frequency range. (b) The identified structural damping: (—∗—), peak band; (—◇—), entire frequency range.

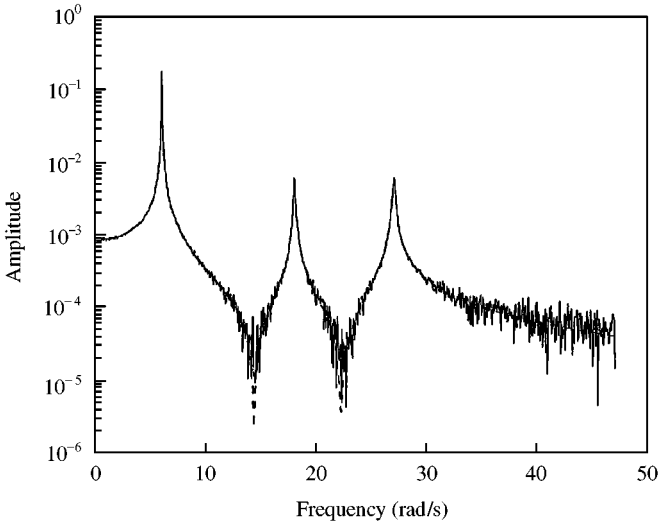

Figure 10. FRF of the system with 0·1% viscous and structural damping and 0·5% noise: (------), without noise; (——), 0·5% noise.

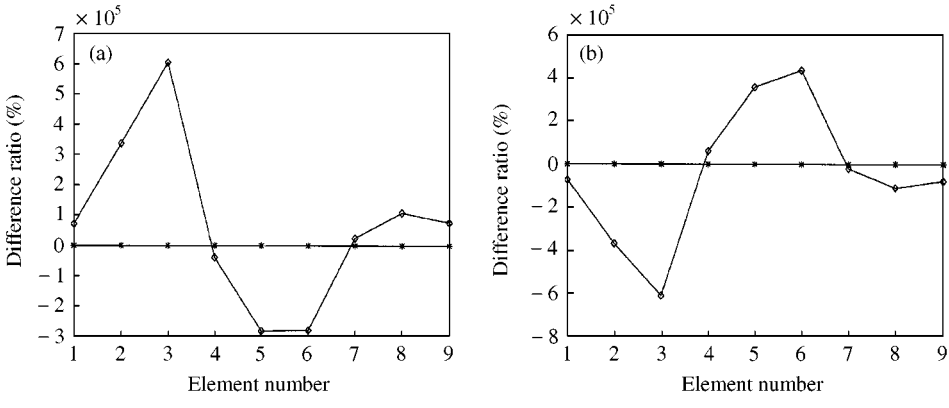

Figure 11. Error ratio diagram of a system with 0·1% damping and 0·5% noise. (a) The identified viscous damping: (—∗—), peak band; (—◇—), entire frequency range. (b) The identified structural damping: (—∗—), peak band; (—◇—), entire frequency range.

not true for the structural damping, because its effect is predominantly in the low-frequency range.

Figure 9 shows the maximum error as defined is about 100% when both the damping ratio and noise are small but of the same order (0·1 and 0·1%). Figures 10 and 11 show the case with 0·1% damping ratio and 0·5% noise level. Figures 12 and 13 show the case with 0·1% damping and 1% noise. As one can see from very large errors in these figures, if the noise is significantly larger than the damping ratio, 5 to 1 and 10 to 1 in these cases, the identification result becomes useless.

In Figures 14 and 15, the damping is large compared to the noise, 0·5% damping and 0·1% noise. In this case, accurate results are obtained with a maximum error less than 10%.

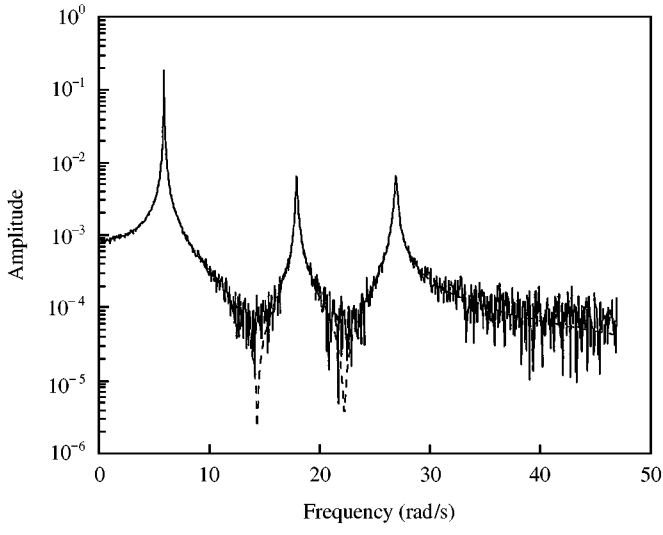

Figure 12. FRF of the system with 0·1% viscous and structural damping and 1·0% noise: (------), without noise; (——), 1·0% noise.

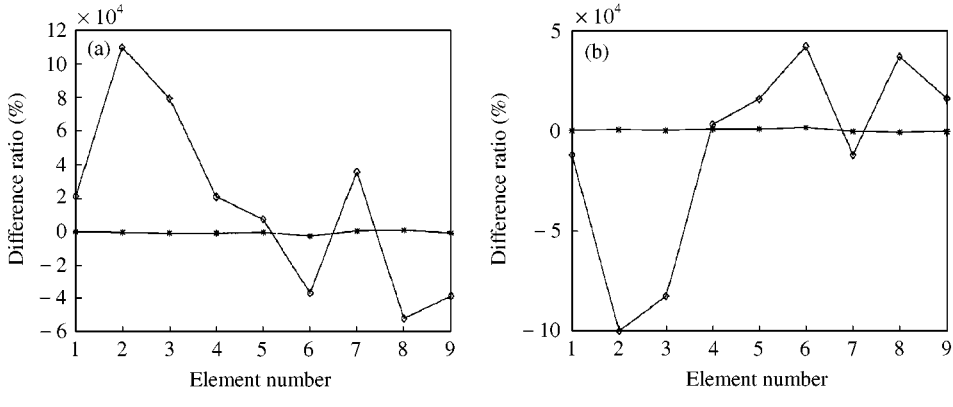

Figure 13. Error ratio diagram of a system with 0·1% damping and 1·0% noise. (a) The identified viscous damping: (—∗—), peak band; (—◇—), entire frequency range. (b) The identified structural damping: (—∗—), peak band; (—◇—), entire frequency range.

Figures 16 and 17 are for the case when both the damping and noise are large but at the same level: 0·5 and 0·5%. The estimation error becomes almost the same order (maximum is about 100%) as the case of Figure 9. Figures 18 and 19 are for the case when the damping is relatively large (0.5%), but the noise is even larger (1%). Again, Figure 19 shows that the identification result contains errors that are too large to be useful. General conclusions can be made from the error study.

- The accuracy of the direct damping identification algorithm developed in this work depends on the magnitude of the noise relative to the damping magnitude. The identification method works accurately if the noise level is the same as or lower than the damping ratio.

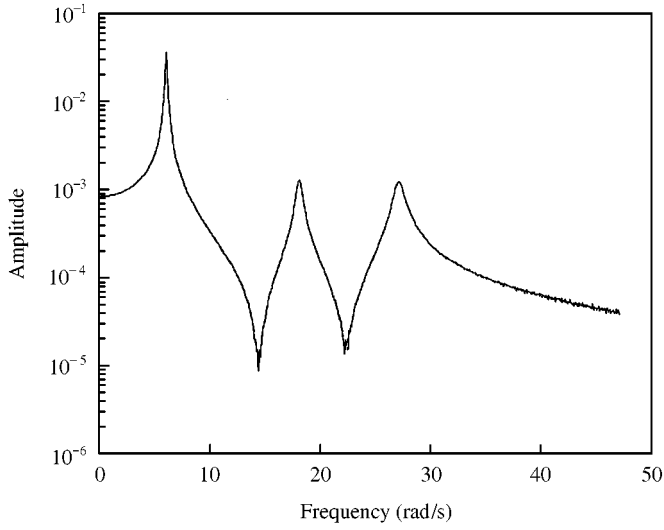

Figure 14. FRF of the system with 0·5% viscous and structural damping and 0·1% noise: (------), without noise; (——), 0·1% noise.

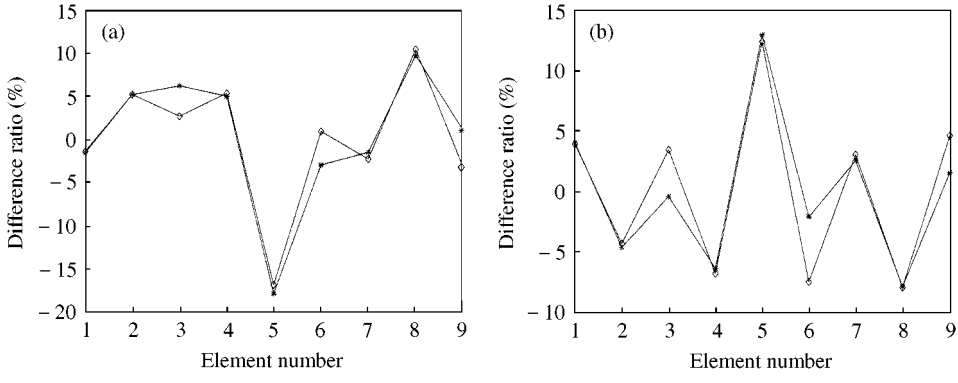

Figure 15. Error ratio diagram of a system with 0·5% damping and 0·1% noise. (a) The identified viscous damping: (—∗—), peak band; (—◇—), entire frequency range. (b) The identified structural damping: (—∗—), peak band; (—◇—), entire frequency range.

- Using the data from FRFs only around the resonance peak improves the accuracy of the identified viscous damping matrix slightly but not the structural damping matrix.

5. EXPERIMENTAL IDENTIFICATION OF DAMPING MATRICES

The damping identification procedure developed in this work was applied to a uniform beam with its ends clamped as shown in Figure 20. Figure 21 shows the schematic diagram of the test rig. The modal test was conducted by the multi-reference impact testing (MRIT) scheme [12, 13] using four acceleration outputs and four impact locations, which results in 16 measured FRFs. Thus, the damping matrices are identified as 4×4 matrices. Each

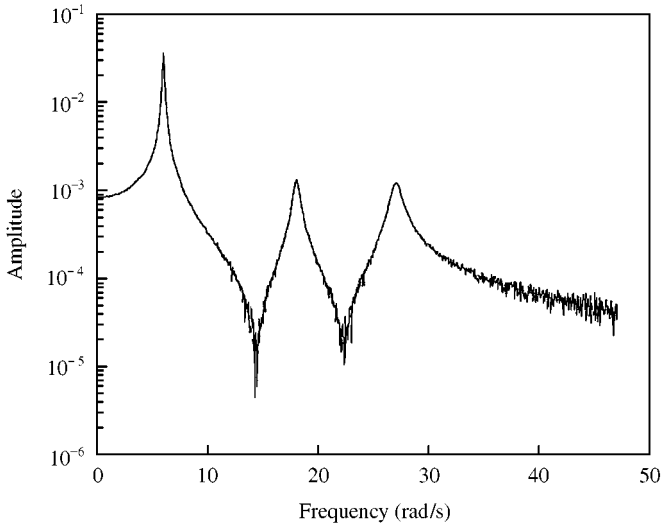

Figure 16. FRF of the system with 0·5% viscous and structural damping and 0·5% noise: (------), without noise; (——), 0·5% noise.

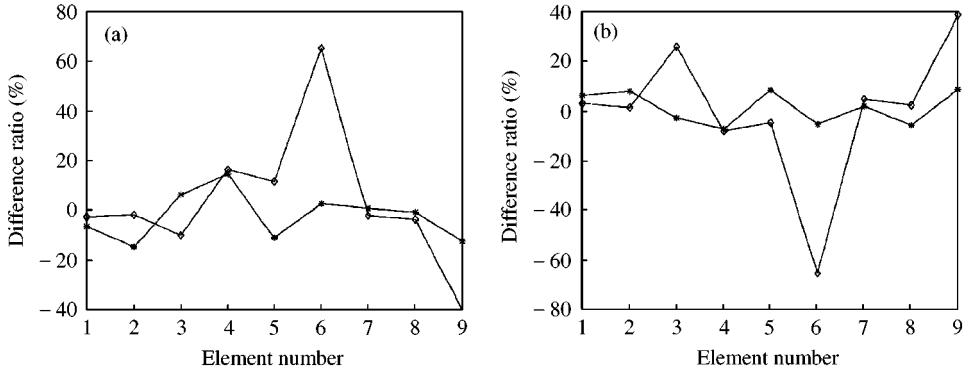

Figure 17. Error ratio diagram of a system with 0·5% damping and 0·5% noise. (a) The identified viscous damping: (—∗—), peak band; (—◇—), entire frequency range. (b) The identified structural damping: (—∗—), peak band; (—◇—), entire frequency range.

impact position is 54 mm apart from each other, which defines the mesh size in the experimental model. The physical properties and dimensions of the beam are listed in Table 4.

5.1. DAMPING MATRICES OF THE BEAM WITHOUT MODIFICATION

The test was done using a single-reed, uniform width beam. Figure 22 shows FRF H_{11}. It shows that the beam has a resonance frequency around 383 Hz, which is very close to the lowest resonance frequency calculated using the Euler beam theory. The identified $[C]$ and $[D]$ matrices are summarized in Table 5. As one can see from the table, the matrices have all

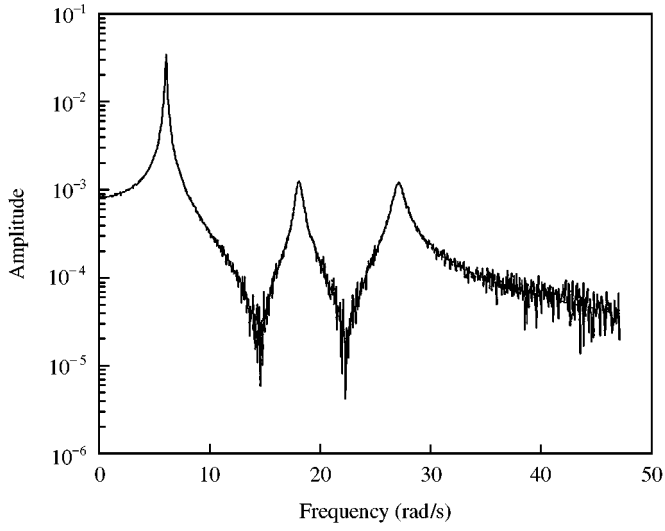

Figure 18. FRF of the system with 0·5% viscous and structural damping and 1·0% noise: (------), without noise; (——), 1·0% noise.

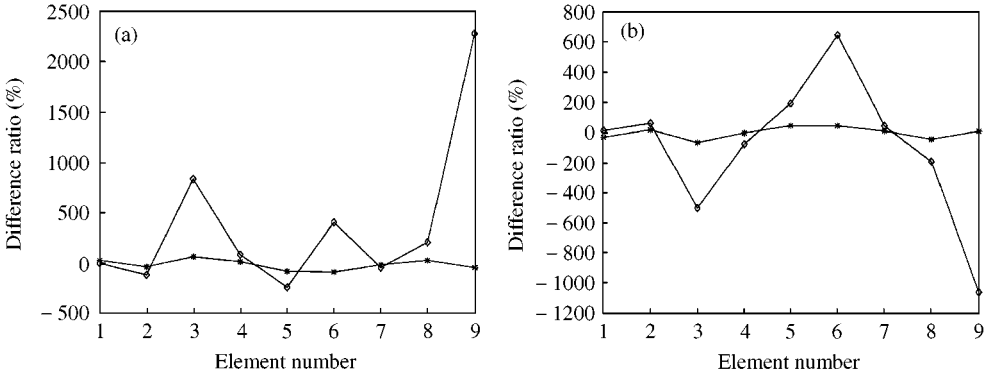

Figure 19. Error ratio diagram of a system with 0·5% damping and 1·0% noise. (a) The identified viscous damping: (—∗—), peak band; (—◇—), entire frequency range. (b) The identified structural damping: (—∗—), peak band; (—◇—), entire frequency range.

the positive diagonal elements as they should. The damping matrices are supposed to be symmetric; however, some deviations are found, which are caused by the experimental errors.

The modal damping ratio of the first mode is found to be 0·65%, therefore the measurement noise should be lower than 0·65%. Although it is not possible to estimate the noise level accurately, an indirect comparison can be made. Comparing the measured FRF in Figure 22 with the theoretical FRFs in Figures 14 (0·5% damping and 0·1% noise) and 16 (0·5% damping and 0·1% noise), it is seen that the measured FRF is cleaner than either of the simulated FRFs, which suggests that the noise level in the experiment is probably lower than 0·1%. Therefore, the measurement noise is believed to be not an issue in this experiment.

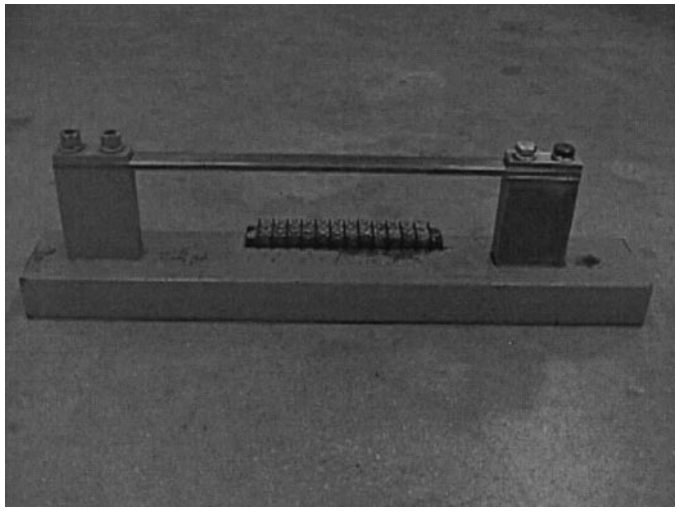

Figure 20. Experimental set-up of the single-reed beam.

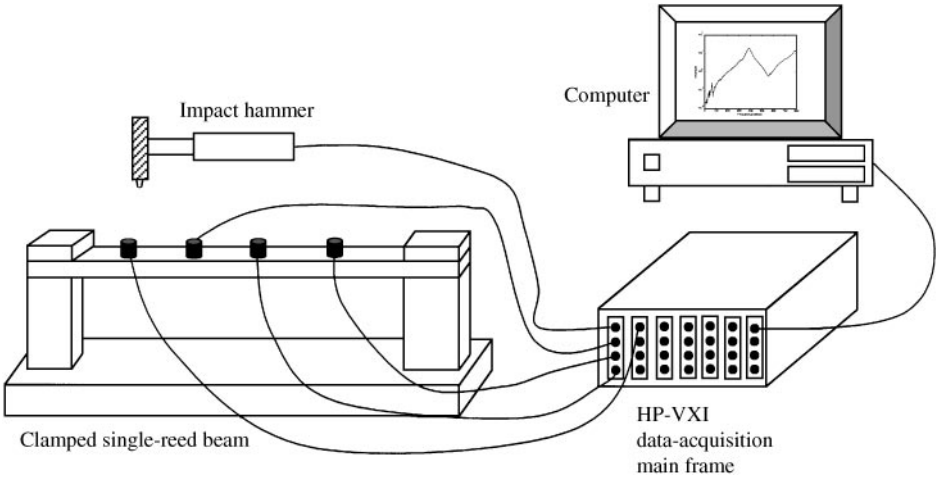

Figure 21. Schematic diagram of the test rig.

TABLE 4

Physical properties and dimensions of the beam tested

Material	Steel	Length (mm)	270·0
Young's modulus (Pa)	$1{\cdot}9 \times 10^{11}$	Width (mm)	19·0
Density (kg/m^3)	7750	Height (mm)	6·0

Figure 23 compares two measured FRFs H_{23} and H_{32}, which have to be the same if the reciprocal theorem is considered; however, they are slightly different from each other. This must have caused the non-symmetry of the off-diagonal terms in the identified damping matrices.

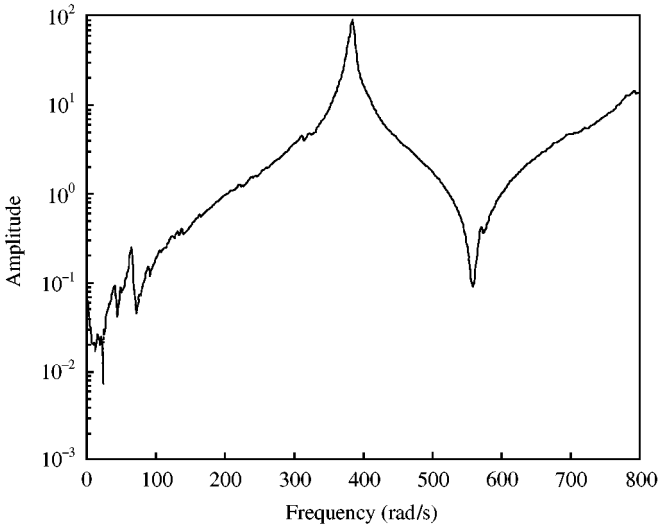

Figure 22. Measured FRF of the single-reed beam.

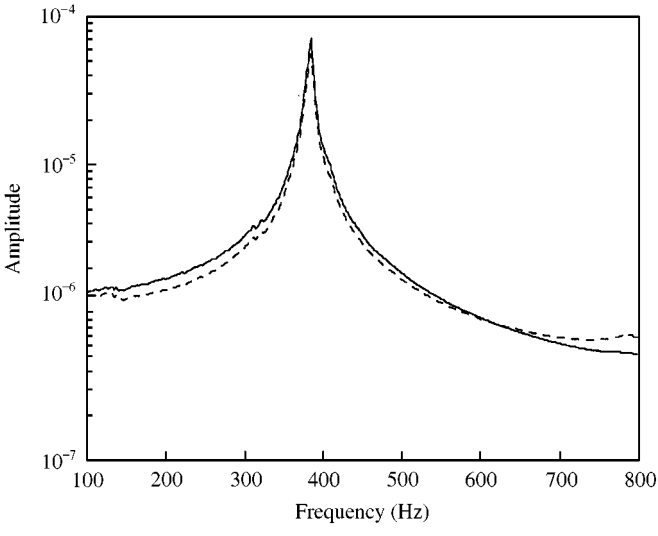

Figure 23. Comparison of measured FRFs: (——), H_{23}; (- - - - -), H_{32}.

5.2. DAMPING MATRICES OF THE BEAM WITH A VISCOUS DAMPER ATTACHED

The experiment was conducted after attaching a small viscous damper to the beam as shown in Figure 24. The damper was attached to a point located 162 mm from the left end of the beam. Figure 25 shows the FRF at the driving point measured at this set-up. In this case, the damping ratio at the first mode is estimated as 3·87%, which means that the measurement noise will not be any problem. The identified $[C]$ and $[D]$ matrices are summarized in Table 5. Again, all diagonal elements are positive and some deviations from the symmetry are found. Compared to the matrices corresponding to the original beam, it is

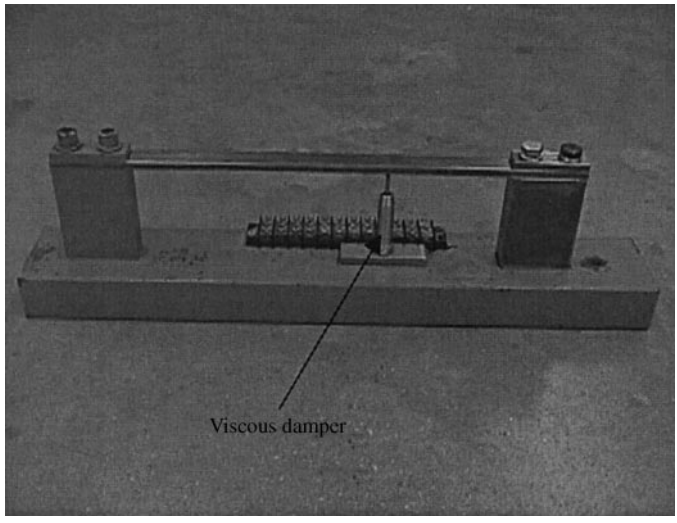

Figure 24. Experimental set-up of the single-reed beam with a viscous damper attached.

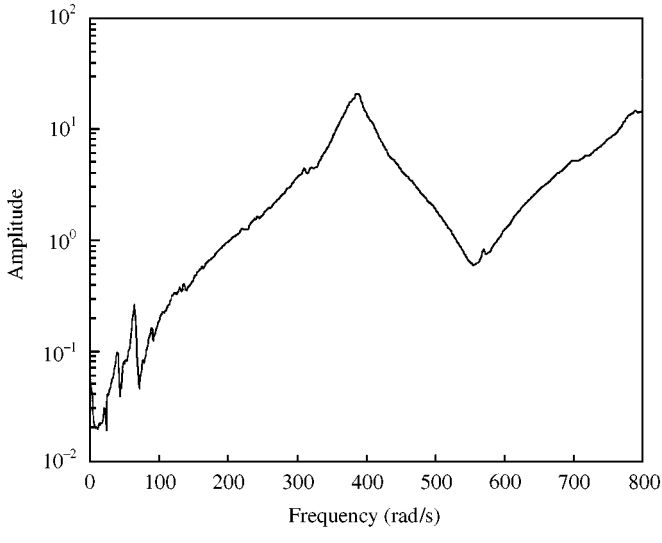

Figure 25. Measured FRF of the single-reed beam with a viscous damper attached.

recognized that the magnitude of the viscous damping matrix is increased significantly as expected.

6. CONCLUSION

A new method for the experimental identification of damping characteristics of a general dynamic system is developed. The method works directly with measured FRFs of the system and identifies different types of damping mechanisms such as the internal structural damping and the external viscous damping in separate matrices. Theoretical validation and error study related to the measurement noise are conducted using a simple 3-d.o.f. system.

TABLE 5

Identified viscous and structural damping matrices of the single-reed beam and the single-reed beam with a viscous damper attached

Single-reed beam				Single-reed beam with a viscous damper attached			
Viscous damping: $[C]$ ($\times 10^4$ (N s/m))							
0·0194	− 0·3084	0·4716	− 0·5095	0·9790	− 4·4694	6·2058	− 5·5155
− 0·1054	0·4633	− 0·6363	0·6238	0·1094	3·8552	− 6·1914	6·6178
0·1840	− 0·5777	0·7484	− 0·6977	− 0·8093	− 3·1790	5·6252	− 6·4731
− 0·2019	0·5438	− 0·6844	0·6376	0·6045	2·7216	− 4·6019	4·9108
Structural damping: $[D]$ ($\times 10^7$ (N/m))							
0·6851	− 1·2381	1·7360	− 2·1633	0·6712	− 0·9244	1·3907	− 2·2416
0·4145	0·4458	− 0·5257	0·7095	− 0·1290	0·0568	− 0·0135	0·0304
0·5428	− 0·4469	0·4182	− 0·6818	0·3866	− 0·2689	0·2788	− 0·6024
− 0·8218	1·4651	− 1·7733	2·0460	− 1·0447	1·5801	− 2·2265	3·4518

The study shows that the method will provide accurate results if the noise level contained in the measured FRFs is equal or lower than the equivalent damping ratio.

The method is applied experimentally to a thin beam with two different configurations. Two distinct configurations used are a single reed, an unmodified beam, a single reed beam with a viscous damper attached. The damping matrices identified reflect the different configurations very well. For example, the magnitudes of the elements of the viscous damping matrix increase in much larger scale compared to those of the structural damping matrix when the viscous damper is attached to the beam.

One of the best applications of the method is considered to be the hybrid modelling of dynamic systems. In the application, the mass and stiffness matrices are formulated using FEM, and the damping matrices are formulated experimentally by the procedure developed in this work. This approach will be very useful to model the complicated realistic systems with hard-to-model energy loss mechanisms.

ACKNOWLEDGMENTS

The authors acknowledge the financial support by ArvinMeritor Industries related to this work.

REFERENCES

1. D. F. PILKEY and D. J. INMAN 1997 *Proceedings of the* 15*th International Modal Analysis Conference*, Orlando, FL. Society for Experimental Mechanics, Inc. 1152–1157. An iterative approach to viscous damping matrix identification.
2. P. LANCASTER 1961 *Journal of the Aerospace Science* **256**. Expression for damping matrices in linear vibration problems.
3. P. EBERSBACH and H. IRRETIER 1989 *American Institute of Aeronautics and Astronautics Journal of Analytical and Experimental Modal Analysis* **4**, 109–116. On the application of modal parameter estimation using frequency domain algorithms.
4. R. J. ALLEMANG and D. L. BROWN 1998 *Journal of Sound and Vibration* **211**, 301–322. A unified matrix polynomial approach to modal identification.

5. Y. G. TSUEI and B. K. HUANG 1998 *Proceedings of the* 16*th International Modal Analysis Conference*, Santa Barbara, CA. Society for Experimental Mechanics, Inc. 1427–1432. Effect of modeling for damping on parameter identification.
6. S. Y. CHEN and Y. G. TSUEI 1997 *Proceedings of the* 15*th International Modal Analysis Conference*, 1139–1144. Effect of parameter identification on modeling of viscous and structural damping.
7. S. Y. CHEN, M. S. JU and Y. G. TSUEI 1996 *American Society of Mechanical Engineers Journal of Vibration and Acoustics* **118**, 78–82. Estimation of mass, stiffness and damping matrices from frequency response functions.
8. ROBERT D. COOK, DAVID S. MALKUS and MICHAEL E. PLESHA 1989 *Concepts and Applications of Finite Element Analysis*. New York: John Wiley and Sons.
9. T. J. YANG 1986 *Finite Element Structural Analysis*. Englewood Cliffs, NJ: Prentice-Hall, 256 pp.
10. D. L. BROWN 1996 *Lecture Notes on Fast Fourier Transform*. University of Cincinnati, SDRL.
11. WILLIAM T. THOMSON and MARIE DILLON DAHLEH 1998 *Theory of Vibration with Applications*. Englewood Cliffs, NJ: Prentice-Hall.
12. R. J. ALLEMANG 1995 *Lecture Notes on Experimental Modal Analysis*. University of Cincinnati, SDRL.
13. R. J. ALLEMANG 1994 *Lecture Notes on Analytical and Experimental Modal Analysis*. University of Cincinnati, SDRL.